Femtosecond Multidimensional Imaging of a Molecular Dissociation

O. Geßner,[1] A. M. D. Lee,[1,2] J. P. Shaffer,[3] H. Reisler,[4] S. V. Levchenko,[4] A. I. Krylov,[4] Jonathan G. Underwood,[5] H. Shi,[6] A. L. L. East,[6] D. M. Wardlaw,[2] E. t. H. Chrysostom,[7] C. C. Hayden,[7] Albert Stolow[1,2]*

The coupled electronic and vibrational motions governing chemical processes are best viewed from the molecule's point of view—the molecular frame. Measurements made in the laboratory frame often conceal information because of the random orientations the molecule can take. We used a combination of time-resolved photoelectron spectroscopy, multidimensional coincidence imaging spectroscopy, and ab initio computation to trace a complete reactant-to-product pathway—the photodissociation of the nitric oxide dimer—from the molecule's point of view, on the femtosecond time scale. This method revealed an elusive photochemical process involving intermediate electronic configurations.

Chemical transformation involves the coupled motions of electrons and nuclei, leading to the flow of both charge and vibrational energy within a reacting molecule. These extremely fast processes can be studied with the use of ultrashort laser pulses, yielding important insights into the underlying dynamics [Nobel Prize lecture by Zewail (1); see also (2)]. One approach to disentangling the intrinsically coupled electronic and vibrational dynamics in excited polyatomic molecules is time-resolved photoelectron spectroscopy (TRPES) (3–5), yielding a picture of both charge and energy flow as a function of time. These measurements, however, are usually made in the laboratory frame, where averaging over the random orientations of the molecule generally leads to a loss of information. Ideally, one would prefer to observe these dynamics from the molecule's point of view rather than the laboratory point of view. One attempt to realize this is to prealign polyatomic molecules before studying their field-free dynamics (6–8). A more general approach is time-resolved coincidence imaging spectroscopy (TRCIS), which measures fully correlated photofragment and photoelectron recoil distributions as a function of time (9, 10), thereby permitting dynamical observations from the molecule's point of view. Here, we used TRPES to measure lifetimes and energetics, combined with TRCIS to measure evolving charge distributions on the molecular frame, to elucidate the dynamics of a complex reaction—the ultraviolet (UV) photodissocia-

tion of the nitric oxide dimer—all the way from initial excitation to final product emission.

The small size and simple cis-planar (C_{2v}) structure of the nitric oxide dimer (NO)$_2$ belies a complex photochemistry (Fig. 1). The broad (190 to 240 nm), featureless UV spectrum (11, 12) arises from a parallel transition to an ill-characterized dissociative continuum (depicted as a gray box). The dissociation yields NO monomer fragments in both the ground [NO(X)] and the first excited [NO(A)] electronic states (13). The NO(A) state has dominant Rydberg 3s orbital character. Unfortunately, neither the featureless absorption spectrum (11, 14) nor the apparently statistical product-state distributions (15, 16) offer much insight into the dynamics. More detailed product-state distributions (17, 18) from (NO)$_2$ excitation just above the NO(A 3s) channel threshold confirm that the photofragment recoil direction is strongly peaked parallel to the pump laser polarization and that the excited molecule retains planar geometry during dissociation. The parallel na-

ture of the optical transition and the fragment recoil direction dictate that the states involved are of B_2 symmetry.

Ab initio studies of the electronically excited dimer states revealed extraordinary complexity, including the existence of low-energy (infrared-resonant) states (19–21). One study established that there exist states in the gray region of Fig. 1 that are of B_2 symmetry; these states consist of a diffuse 3p$_y$ Rydberg state (y axis along the N-N bond) and a localized valence state that carries the oscillator strength (22, 23). Photofragment indistinguishability permits both in-phase and out-of-phase combinations of [NO(A 3s) + NO(X)] with [NO(X) + NO(A 3s)] products. As shown in Fig. 2, for C_{2v} geometry the in-phase combination would produce a dimer Rydberg 3s state of A_1 symmetry, whereas the out-of-phase combination would produce a dimer Rydberg 3p$_y$ state of B_2 symmetry (where y is along the N-N bond).

Our experimental methods were as described (9, 24). Briefly, a supersonic molecular beam source (15% NO in He) produced cold (NO)$_2$, which was pumped with femtosecond pulses at 209.6 nm and probed, via single-photon ionization, with femtosecond pulses at 279.5 nm. The time resolution (i.e., instrumental response function or "cross-correlation") was 160 ± 10 fs. The pump and probe laser polarizations were parallel to each other. The dynamics were monitored in two independent experiments. High-resolution time- and energy-resolved spectra were recorded with TRPES, whereas three-dimensional (3D) energy- and angle-resolved photoelectron-photoion correlations were measured with TRCIS at five specific time delays.

TRPES tracks the evolving excited state all the way from initial excitation ($\Delta t = 0$) to final
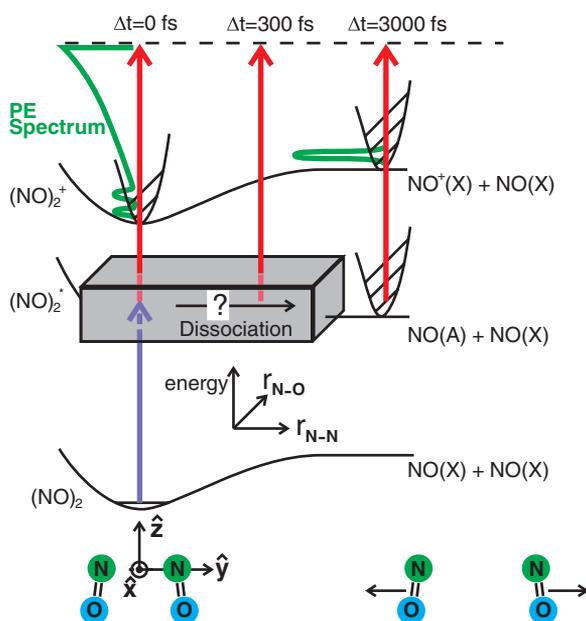
[1]Steacie Institute for Molecular Sciences, National Research Council Canada, Ottawa, Ontario K1A 0R6, Canada. [2]Department of Chemistry, Queen's University, Kingston, Ontario K7L 3N6, Canada. [3]Department of Physics and Astronomy, University of Oklahoma, Norman, OK 73019, USA. [4]Department of Chemistry, University of Southern California, Los Angeles, CA 90089, USA. [5]Department of Physics and Astronomy, Open University, Milton Keynes MK7 6AA, UK. [6]Department of Chemistry, University of Regina, Regina, Saskatchewan S4S 0A2, Canada. [7]Combustion Research Facility, Sandia National Laboratories, Livermore, CA 94551, USA.

*To whom correspondence should be addressed. E-mail: albert.stolow@nrc.ca

Fig. 1. Schematic representation of the femtosecond pump-probe TRPES study of the NO dimer dissociation dynamics. The gray box represents the complex region the molecule must pass through upon UV photodissociation into NO(A) + NO(X). The TRPES method monitors the complete time evolution of the excited state. Our molecular frame axis convention is shown (bottom), with the y axis along the N-N bond. The purple arrow represents the pump (excitation) laser photon. The red arrows represent the probe (ionization) laser photon that interrogates the evolving excited state, shown here at three selected time delays. The green curves represent the photoelectron kinetic energy (PE) spectrum observed after ionization at these time delays.

Fig. 2. A depiction of the consequences of photofragment indistinguishability. Quantum mechanically, the product states are linear combinations of [NO(X) + NO(A)] with [NO(A) + NO(X)]. As shown, the in-phase combination would correlate with an A_1 symmetry 3s Rydberg dimer state, whereas the out-of-phase combination would correlate with a B_2 symmetry 3p$_y$ Rydberg dimer state (where y is the N-N bond axis). Our results indicate that the participating state is the (NO)$_2$ Rydberg 3p$_y$ state.
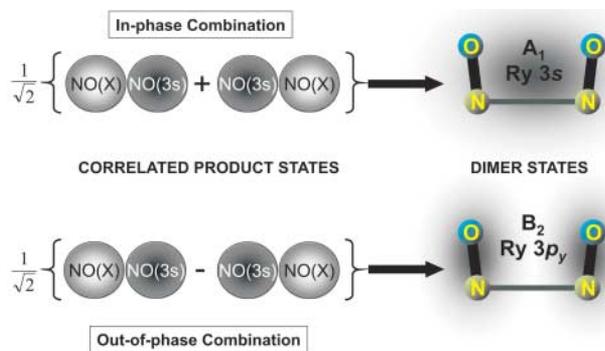
Fig. 3. A TRPES scan showing photoelectron spectra as a function of time delay in a 2D plot. The binding energy is the total photon energy (pump plus probe) minus the electron kinetic energy. The green insets (top) are examples of photoelectron spectra at two time delays. The blue insets (bottom) are examples of the evolution of the photoelectron intensity at two binding energies. Note that the 2D data are globally fit at all energies and time delays simultaneously. The solid lines in the blue graphs are from the 2D fits to a sequential two-step dissociation model. The dotted lines are the respective initial-, intermediate-, and final-state signal components plus a small instrumental response contribution.
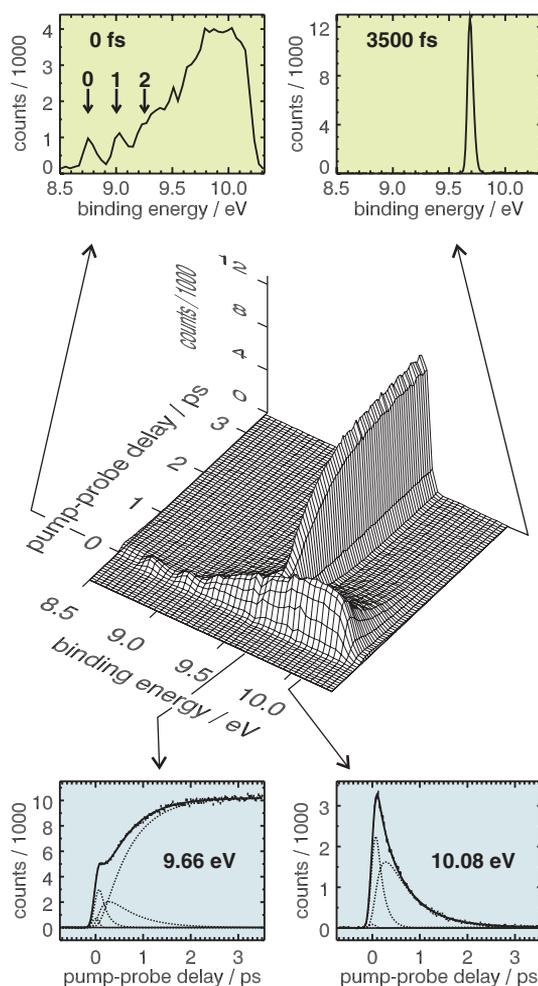
products ($\Delta t > 3000$ fs), illuminating the obscure gray region in Fig. 1. Previous TRPES studies investigated the NO(A 3s) channel, revealing that the products emerge on the sub-picosecond time scale (*25–28*). An early study proposed a two-step nonadiabatic mechanism (*25*), whereas later work favored a more direct process via a dimer 3s Rydberg state (*26–28*).

The 2D plot in Fig. 3 shows TRPES spectra of (NO)$_2$ from initial excitation to final dissociation. Cuts parallel to the binding energy axis yield the photoelectron spectrum at given time delays (green insets). Cuts parallel to the pump-probe time delay axis reveal the evolution of a given photoelectron band (blue insets). At $\Delta t = 0$, a broad spectrum due to photoionization of (NO)$_2$* shows two resolved peaks assigned to 0 and 1 quanta of the cation N=O symmetric stretch mode (v_1). The $v_1 = 2$ peak merges with a broad, intense Franck-Condon dissociative continuum. (Note that $v_1 = 3$ would be above the dissociation limit of the dimer

cation.) That this broad continuum dominates the spectrum shows that (NO)$_2$* photoionization favors dissociation of the dimer. By contrast, single-photon ionization of the ground state does not (*29*), which suggests that (NO)$_2$* is geometrically distorted with respect to both the neutral and cation ground states.

At long times ($\Delta t = 3500$ fs), we see the sharp photoelectron spectrum of the free NO(A 3s) product. The 10.08-eV band shows the decay of the (NO)$_2$* excited state. The 9.66-eV band shows both the decay of (NO)$_2$* and the growth of free NO(A 3s) product. To extract dynamical information, we used nonlinear fitting procedures to globally fit the complete 2D data of Fig. 3 at all photoelectron energies and time delays simultaneously.

These data cannot be fit by single-exponential kinetics. They are fit with high accuracy by a two-step sequential model, meaning that an initial bright state (NO)$_2$* evolves to an intermediate configuration, which itself subsequently decays to yield free NO(A 3s) products. The evidence most strongly supporting the intermediate configuration is seen in the 9.66-eV electron band, showing product growth. The delayed rise of the free NO(A 3s) product cannot be fit by a single-exponential decay followed by single-exponential growth with the same time constant. The 10.08-eV dissociative ionization band, dominant at early times, is revealing of (NO)$_2$* configurations preceding dissociation. As seen in Fig. 3, its time evolution, which cannot be fit by a single-exponential decay, provides another clear view of the intermediate step.

We conclude that only two time constants in a sequential model are required to very accurately fit these 2D data at all photoelectron energies and all time delays simultaneously. The decay time of the initial state is 140 ± 30 fs, which matches the rise time of the intermediate configuration. This intermediate configuration has a subsequent decay time of 590 ± 20 fs. These two time constants result in a maximum for the intermediate configuration signal at ~330 fs delay. The two components can be seen as the dotted lines in the fits to the 10.08-eV data (along with a small instrumental response signal). In the 9.66-eV band, the dotted lines from the fits show that the rise of the NO(A 3s) product channel is first delayed by 140 ± 30 fs but then grows with a time constant of 590 ± 20 fs. We emphasize that although only two cuts are shown, the data are fit at all time delays and photoelectron energies simultaneously (*30*). In sum, we show clear evidence for an intermediate configuration in (NO)$_2$ UV photodissociation.

To identify this intermediate configuration, we applied the TRCIS method, which records the 3D recoil momentum vectors of both photoelectrons and photoions in coincidence (*9*). This 6D fully correlated data set may be cut, projected, or filtered to reveal both scalar and

vector correlations as a function of time. We restrict our discussion here to angular correlations.

The pump transition dipole is along the molecular frame y axis, the N-N bond axis (see Fig. 1). The pump transition therefore forms an anisotropic distribution of excited $(NO)_2^*$ states in the lab frame, with the N-N bond aligned along the laser polarization axis. As we are concerned with intermediate configurations in $(NO)_2^*$ evolution, we consider the photoionization probing of $(NO)_2^*$, which leads predominantly to dissociative ionization (Fig. 3). Dissociative photoionization has long been recognized as a route to recoil or molecular-frame photoelectron angular distributions in non–time-resolved studies (31, 32). The dissociative ionization of $(NO)_2^*$ produces NO^+ fragments strongly directed along the laser polarization axis. The NO^+ fragment recoil direction therefore indicates the lab frame direction of the N-N bond (molecular frame y axis) before ionization. Rotating the electron momentum vector into the fragment recoil frame on an event-by-event basis allows for reconstruction of the $(NO)_2^*$ photoelectron angular distribution in this recoil frame, rather than the usual lab frame. Here the recoil frame coincides with the molecular frame, differing only by azimuthal averaging about the N-N bond. Out of all fragment recoil events, we selected only those directed ("up" or "down") along the parallel pump and probe laser polarization axis. By choosing events from this selected set, we restrict the data to excited-state ionization events arising from interactions with the y component of the ionization transition dipole. This restriction greatly limits the allowed partial waves for the emitted electron, especially in the present case where only a single electronic continuum is accessed (30).

In Fig. 4 we present time-resolved lab and recoil frame photoelectron angular distributions arising from photoionization of $(NO)_2^*$ in the 9.9- to 10.3-eV band of Fig. 3. As can be seen, this dissociative ionization region contains significant contributions from the intermediate configuration. In general, the time dependence of photoelectron angular distributions is related to the evolution of excited-state electronic structure (5, 33–35). Here, the lab frame photoelectron angular distributions have a largely isotropic character that shows little time evolution, obscuring information about excited-state dynamics. By contrast, the recoil frame photoelectron angular distributions show a highly anisotropic character and a variation with time delay. The solid lines in the polar plots of Fig. 4 are fits to Legendre polynomials (36).

The recoil frame photoelectron angular distributions have dominant intensity perpendicular to the laser polarization axis. An A_1 Rydberg 3s intermediate state would most likely yield maximum intensity parallel to the laser polarization axis, contrary to what is observed. This rules out the A_1 Rydberg 3s state
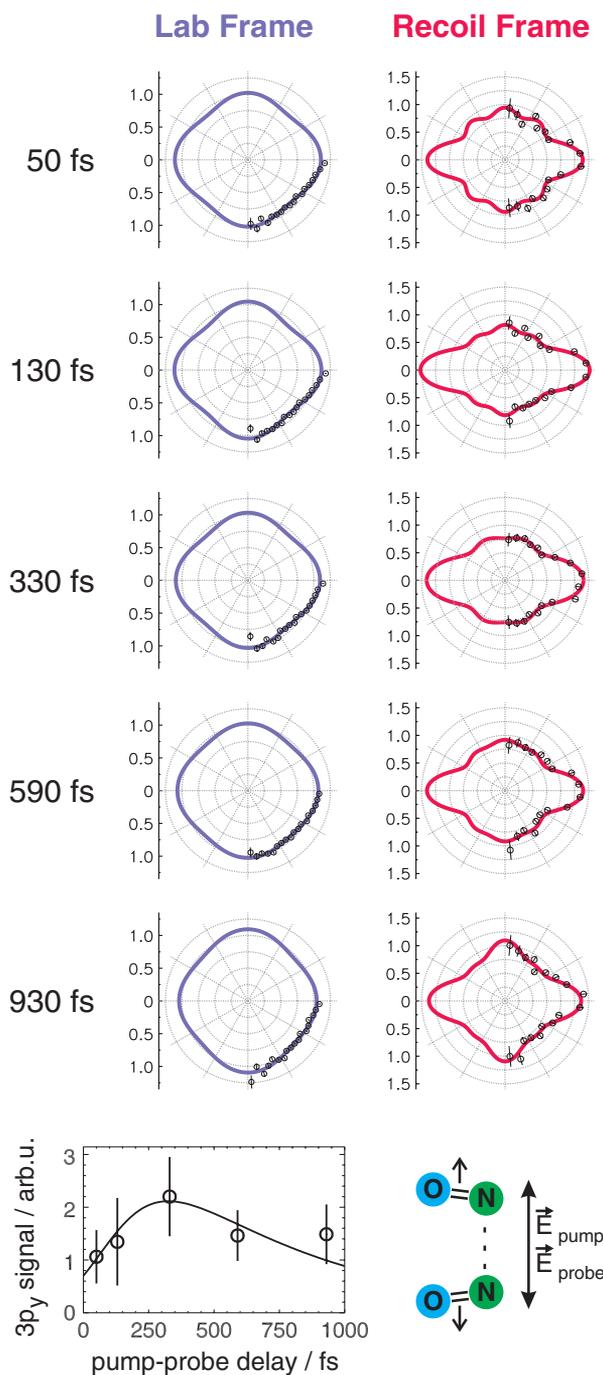
as the intermediate configuration. We used states of B_2 symmetry to model the recoil frame photoelectron angular distributions, a choice corroborated by our ab initio calculations. We also presumed that the molecule largely retains C_{2v} symmetry, an assumption consistent with the observed retention of planarity during dissociation (17).

Proceeding further required a detailed analysis of the photoelectron angular distributions (36). The outgoing free electrons are described in terms of their angular momenta by the so-called partial waves, using spherical harmonics labeled by the quantum numbers l and m. For

example, in the atomic limit, a Rydberg p-state would produce s and d partial waves upon single-photon ionization ($\Delta l = \pm 1$). In the molecular case, we decompose the free-electron wave function into symmetry-adapted spherical harmonics (35). For C_{2v}, these harmonics are described by their C_{2v} symmetry and by $l_{|\lambda|}$, where l and $|\lambda|$ are the orbital angular momentum and projection quantum numbers, respectively. Values of $l = 0, 1, 2\ldots$ are labeled s, p, d, …, whereas values of $|\lambda| = 0, 1, 2, \ldots$ are labeled $\sigma, \pi, \delta, \ldots$ In our case, ionization of a B_2 electronic state to an A_1 cation state via a y-polarized transition means that the free

Fig. 4. A TRCIS study showing lab frame (**left**) and recoil frame (**right**) photoelectron angular distributions (PADs) from the 9.9- to 10.3-eV dissociative ionization region of Fig. 3. The laser polarizations and recoil frame axes are along the y direction, as shown (**bottom right**). The lab frame PADs show featureless and almost invariant behavior. The recoil frame PADs show strong anisotropies that vary with time. The fit curves (solid lines) include even-order Legendre polynomials P_L up to $L = 4$ for the lab frame and up to $L = 8$ for the recoil frame. The average partial wave contribution expected from Rydberg $3p_y$ ionization is plotted at the lower left as a function of time. The time dependence of the intermediate configuration extracted from Fig. 3 is plotted here as the solid line, agreeing well with the time dependence of the $3p_y$ ionization contribution. This confirms the intermediate configuration as being of Rydberg $3p_y$ character.

electron must have A_1 symmetry, significantly restricting the allowed free-electron states. The A_1 symmetry partial waves are s_σ, p_σ, d_σ, d_δ, f_σ, f_δ, g_σ, g_δ, and g_γ. Our modeling of the data is not unique, and the individual partial wave contributions varied depending on the model input parameters. In general, the s, p, and d partial waves were dominant. To obviate the dependence of our conclusions on any specific partial wave amplitude, we contracted the amplitudes into two sets: those expected from $3p_y$ ionization and those not. Ionization of a dimer $3p_y$ Rydberg state via a y-polarized transition would produce only electrons with s_σ, d_σ, and d_δ character. Therefore, the ratio of $(s_\sigma + d_\sigma + d_\delta)$ to the sum of all other contributions Σ_{pfg} is a measure of $3p_y$ Rydberg character in the $(NO)_2^*$ excited electronic states. At the bottom of Fig. 4 we plot the time dependence of this ratio, labeled "$3p_y$ signal"; this plot shows that dimer $3p_y$ Rydberg character rises from early times, peaks at ~330 fs, and subsequently falls. The solid curve is the time dependence of the intermediate configuration extracted from Fig. 3, showing that the $3p_y$ character follows the time behavior of the intermediate configuration. The agreement substantiates the intermediate configuration as being of $3p_y$ character.

Our ab initio studies fully support this picture (36). Briefly, a very bright diabatic charge transfer (valence) state carries the transition oscillator strength. At our pump photon energy, a vibrationally excited (we roughly estimate $v_1 \sim 4$) adiabatic $(NO)_2^*$ state of mixed charge-transfer/Rydberg character is populated. This quickly evolves, via N=O stretch dynamics, toward increasing $3p_y$ Rydberg character. The 140-fs initial decay constant is the time scale for the initial valence state to develop intermediate $3p_y$ character and explains the emergence of $3p_y$ ionization dynamics seen in Fig. 4 at intermediate time scales. The 590-fs sequential time constant is the time scale for evolution of the dimer $3p_y$ configuration to free products via intramolecular vibrational energy redistribution, coupling the N=O stretch to the low-frequency N-N stretch (37). The dimer $3p_y$ state adiabatically correlates to free NO(A 3s) + NO(X) products. Finally, a dimer A_1 Rydberg 3s state was found at lower energy than the bright valence state but does not cross the latter in the Franck-Condon region.

The dynamics of excited polyatomic molecules generally involves the complex mixing of electronic states. Here we studied the case of Rydberg-valence mixing in a molecular dissociation, a situation found in the photochemistry of higher excited states of molecules. By placing ourselves in the frame of the molecule, we are able to observe new details of the evolution of the electronic states that cannot be extracted from lab frame measurements alone. We expect that multidimensional femtochemistry, seen from the molecule's point of view, will shed light on the dynamical evolution of increasingly complex chemical processes.

References and Notes

1. A. H. Zewail, *Angew. Chem. Int. Ed.* **39**, 2586 (2000).
2. A. Stolow, D. M. Jonas, *Science* **305**, 1575 (2004).
3. V. Blanchet, M. Z. Zgierski, T. Seideman, A. Stolow, *Nature* **401**, 52 (1999).
4. A. Stolow, *Annu. Rev. Phys. Chem.* **54**, 89 (2003).
5. A. Stolow, A. E. Bragg, D. M. Neumark, *Chem. Rev.* **104**, 1719 (2004).
6. H. Stapelfeldt, T. Seideman, *Rev. Mod. Phys.* **75**, 543 (2003).
7. J. G. Underwood, B. J. Sussman, A. Stolow, *Phys. Rev. Lett.* **94**, 143002 (2005).
8. T. P. Rakitzis, A. J. van den Brom, M. H. M. Janssen, *Science* **303**, 1852 (2004).
9. J. A. Davies, J. E. LeClaire, R. E. Continetti, C. C. Hayden, *J. Chem. Phys.* **111**, 1 (1999).
10. J. A. Davies, R. E. Continetti, D. W. Chandler, C. C. Hayden, *Phys. Rev. Lett.* **84**, 5983 (2000).
11. J. Billingsley, A. B. Callear, *Trans. Faraday Soc.* **67**, 589 (1971).
12. E. Forte, H. van den Berg, *Chem. Phys.* **30**, 325 (1978).
13. O. Kajimoto, K. Honma, T. Kobayashi, *J. Chem. Phys.* **89**, 2725 (1985).
14. V. Dribinski, A. B. Potter, I. Fedorov, H. Reisler, *Chem. Phys. Lett.* **385**, 233 (2004).
15. Y. Naitoh, Y. Fujimura, K. Honma, O. Kajimoto, *Chem. Phys. Lett.* **205**, 423 (1993).
16. Y. Naitoh, Y. Fujimura, K. Honma, O. Kajimoto, *J. Phys. Chem.* **99**, 13652 (1995).
17. A. V. Demyanenko, A. B. Potter, V. Dribinski, H. Reisler, *J. Chem. Phys.* **117**, 2568 (2002).
18. A. B. Potter, V. Dribinski, A. V. Demyanenko, H. Reisler, *J. Chem. Phys.* **119**, 7197 (2003).
19. A. L. L. East, *J. Chem. Phys.* **109**, 2185 (1998).
20. R. Sayos, R. Valero, J. M. Anglada, M. Gonzalez, *J. Chem. Phys.* **112**, 6608 (2000).
21. M. Tobita *et al.*, *J. Chem. Phys.* **119**, 10713 (2003).
22. S. V. Levchenko, A. I. Krylov, as reported in (14).
23. Our C_{2v}, y axis lies along the N-N bond, following Herzberg's convention. Our earlier paper (14) used the alternate convention, and there the N-N bond was called the x axis. No conclusions depend on the axis convention used.
24. S. Lochbrunner *et al.*, *J. Electron Spectrosc. Relat. Phenom.* **112**, 183 (2000).
25. V. Blanchet, A. Stolow, *J. Chem. Phys.* **108**, 4371 (1998).
26. M. Tsubouchi, C. A. de Lange, T. Suzuki, *J. Chem. Phys.* **119**, 11728 (2003).
27. M. Tsubouchi, T. Suzuki, *Chem. Phys. Lett.* **382**, 418 (2003).
28. M. Tsubouchi, C. A. de Lange, T. Suzuki, *J. Electron Spectrosc. Relat. Phenom.* **142**, 193 (2005).
29. F. Carnovale, J. B. Peel, R. G. Rothwell, *J. Chem. Phys.* **84**, 6526 (1986).
30. The amplitudes of all fit functions vary smoothly and continuously as a function of electron kinetic energy. This absence of any threshold effects suggests that all ionization is into the electronic continuum of the $^2A_1$ dimer cation ground state. Indeed, our ab initio calculations show that the configurations involved in the UV-excited NO dimer states contain only single electron excitations. The Koopmans' ionization correlations for these UV states would therefore be to the ground electronic state of the cation, consistent with our observations.
31. J. H. D. Eland, *J. Chem. Phys.* **70**, 2926 (1979).
32. K. G. Low, P. D. Hampton, I. Powis, *Chem. Phys.* **100**, 401 (1985).
33. T. Seideman, *Annu. Rev. Phys. Chem.* **53**, 41 (2002).
34. K. L. Reid, *Annu. Rev. Phys. Chem.* **54**, 397 (2003).
35. K. L. Reid, J. G. Underwood, *J. Chem. Phys.* **112**, 3643 (2000).
36. See supporting material on *Science* Online.
37. O. Gessner *et al.*, in preparation.
38. Supported by the Natural Sciences and Engineering Research Council of Canada (A.M.D.L., D.M.W., A.L.L.E., and A.S.), NSF (H.R., A.I.K.), and the U.S. Department of Energy, Office of Basic Energy Science, Division of Chemical Sciences, Geosciences, and Biosciences (C.C.H.).

A Bacterial Inhibitor of Host Programmed Cell Death Defenses Is an E3 Ubiquitin Ligase

Radmila Janjusevic,[1]* Robert B. Abramovitch,[2,3]* Gregory B. Martin,[2,3]† C. Erec Stebbins[1]†

The *Pseudomonas syringae* protein AvrPtoB is translocated into plant cells, where it inhibits immunity-associated programmed cell death (PCD). The structure of a C-terminal domain of AvrPtoB that is essential for anti-PCD activity reveals an unexpected homology to the U-box and RING-finger components of eukaryotic E3 ubiquitin ligases, and we show that AvrPtoB has ubiquitin ligase activity. Mutation of conserved residues involved in the binding of E2 ubiquitin–conjugating enzymes abolishes this activity in vitro, as well as anti-PCD activity in tomato leaves, which dramatically decreases virulence. These results show that *Pseudomonas syringae* uses a mimic of host E3 ubiquitin ligases to inactivate plant defenses.

Type III secretion systems (T3SS) translocate bacterial virulence proteins into host cells to modulate diverse eukaryotic biochemical processes (1–5). *Pseudomonas syringae* pathovar (pv.) *tomato* DC3000 causes disease in tomato and *Arabidopsis* and uses a T3SS to evade the host's programmed cell death (PCD) response, which sacrifices a limited portion of the plant to protect the rest from systemic infection (6). The *Pseudomonas syringae* type III effector AvrPtoB is delivered into plant cells, where it elicits a host response that varies for resistant and susceptible tomato lines (7). In resistant plants, AvrPtoB is rec-